Preprint
UCRL-ID-151943

Development of Solid State NMR Methods for the Structural Characterization of Membrane Proteins: Applications to Understand Multiple Sclerosis

M. Cosman, A-T. Tran, J. Ulloa, and R. S. Maxwell

U.S. Department of Energy
Lawrence Livermore National Laboratory

March 4, 2003

DISCLAIMER

This work was performed under the auspices of the U. S. Department of Energy by the University of California, Lawrence Livermore National Laboratory under Contract No. W-7405 Eng.-48

01-LW-066

DEVELOPMENT OF SOLID STATE NMR METHODS FOR THE STRUCTURAL CHARACTERIZATION OF MEMBRANE PROTEINS: APPLICATIONS TO UNDERSTAND MULTIPLE SCLEROSIS.

Final Report

Monique Cosman, Anh-Truet Tran, Josh Ulloa, and Robert S. Maxwell

Abstract: Multiple sclerosis (MS) is a relapsing-remitting disorder of the central nervous system that results in the loss of the myelin sheaths insulating nerve fibers (axons). Strong evidence suggests that MS is an autoimmune disease mediated by T-cell and antibody responses against myelin antigens. Myelin oligodendrocyte glycoprotein (MOG) is a 26 kD to 28 kD an integral membrane protein of the central nervous system implicated as a target for autoaggressive antibodies in MS. To date, the conformation of MOG in association with the myelin membrane is unknown and the exact nature of the interactions between this protein and disease-inducing immune responses have not been determined. Since membrane associated proteins are typically characterized by decreased correlation times, solution state NMR methodologies are often impracticable. Membrane proteins are also often difficult to crystallize for X-ray diffraction studies. Consequently, there is an urgent need to develop new structure characterization tools for this important class of biomolecules. The research described here overviews the initial stages of our effort to develop an integrated, NMR based approach to structural studies of MOG over the many structural domains it is postulated to posess. The structural knowledge gained about this important MS antigen in its native environment will contribute significantly to our understanding of its function *in vivo*. This project will also aid in the development of therapeutics to inhibit the antigen/antibody interaction and thus prevent demyelination in MS patients.

Introduction

Multiple Sclerosis is a chronic, relapsing-remitting disorder of the central nervous system (CNS) white matter that results in the loss of the myelin sheaths insulating nerve fibers (demyelination) (*1*). Similarities to the disease model experimental allergic encephalomyelitis (EAE) and strong circumstantial evidence suggest that human MS is mediated by autoagressive immune responses directed against CNS myelin (*2-4*). EAE is an autoimmune, inflammatory CNS disorder that is induced in susceptible strains of laboratory animals by sensitization against various myelin components (*5, 6*). Recent studies suggest complex, and/or multiple pathophysiologic mechanisms for autoimmune demyelinating disorders, a concept supported by the various patterns of myelin destruction encountered in MS and the many different existing models of EAE (*7, 8*). In particular, the balance between T cell and antibody responses, which may be directed against multiple myelin antigens, appears to influence the respective magnitude of infiltration by inflammatory cells and demyelination observed in CNS lesions (*9*).

A significant obstacle to understanding human MS is that to date, the target antigens in MS have not been unequivocally identified, with the exception of a small myelin protein named myelin oligodendrocyte glycoprotein (MOG). The MOG antigen is unique among myelin proteins because it appears capable of inducing MS-like, demyelinating forms of EAE in all laboratory species and strains, including non-human primates (*10-13*). Strong T cell and humoral (antibody) responses directed against MOG have also been demonstrated in humans (*14-17*). Importantly, autoimmunity against MOG includes a pathogenic humoral component, with the production of MOG-specific antibodies that have the potential to worsen EAE and are directly responsible for the demyelination in several species (*13, 18, 19*). Among species susceptible to sensitization with MOG(1-117) is the *Callithrix jacchus* (*C. jacchus*) marmoset, a small outbred non human primate raised in captivity which typically develops a form of EAE that faithfully recapitulates clinical and pathological features of human MS (*13, 32*). In both acute forms of MS and MOG-induced marmoset EAE, actively demyelinating lesions display a characteristic structural pattern of myelin destruction where the compact myelin undergoes vesicular disruption. This dramatic transformation appears to follow the

formation of large intramyelinic vacuoles and is associated with the binding of MOG-specific autoantibodies (*33*).

MOG is a quantitatively minor (0.01% to 0.05%) CNS membrane protein (*20*) comprised of 218 amino acid residues and is found primarily on the extracellular surface of oligodendrocytes in the outermost lamellae of the myelin sheath, which may explain its accessibility to antibody attack in MS and EAE (*21, 22*), (for a recent review, see Johns and Bernard (*23*)). The function of MOG is unknown and there are no crystal or high-resolution NMR structures available. Based on existing models and hydrophobicity studies (*26, 27*), it appears to be comprised of an immunoglobulin-like N-terminal extracellular domain (residues 1-121) and a hydrophobic domain (residues 122-218). The topology of the hydrophobic domain is believed to consist of a single transmembrane spanning segment (residues 122-150), and a C-terminal segment (residues 174-200), that may be semi-embedded in the myelin bilayer with the C-terminus tail intracellularly located (see Figure 2). The nonglycosylated, recombinant N-terminus domain of MOG (MOG(1-117)) suffices for sensitizing animals for EAE (*11-13, 28-31*).

Motivation

Membrane proteins comprise approximately 30% of cellular proteins and are involved in critical functions such as signaling (communication between cells) and mediating cell transport (including toxins). Unfortunately, currently available methods are inadequate in determining the structures of membrane proteins and thus structure/function studies of this class of biomolecules are lagging behind those for their aqueous soluble counterparts. The research described here directly addresses this issue by the development of a new integrated NMR based approach to study membrane proteins, such as MOG, that posess both cellular and extracellular domains. In addition to NMR methods, we have also applied traditional biological and biochemical methods for the preparation, purification, and structural screening of MOG. These methods include homology modeling, activity testing, and circular dichroism. The approach outlined below will allow us to develop and test general experimental strategy for the structural

characterization of membrane bound proteins, an important class of biomolecules that has proven to be difficult to study by other methods.

Successful demonstration of our methodology to determine the structure of MOG will specifically be of great importance for the understanding its function and for the development of therapeutics for the treatment of MS. Due to the extensive biochemical, biocomputational, and bioanalytical capabilities, including solid-state NMR, LLNL is uniquely suited to investigate this important problem. Further, if successful, the methods we will develop in this project will have significant impact on fundamental biochemical R&D processes ongoing at LLNL, including the development of molecular biosensors for the detection of toxins and other biowarfare agents. Due to the extensive experience in its biochemistry, MOG is being used as a model system to validate our methodology for application to a large variety of potential applications.

Experimental

Development of Homology Model: The methods to predict initial structural models of MOG from multiple species are described in detail in Mesleh, et al 2002 [105]. Some of the results from the modeling study are shown in Figure 2.

Expression and Purification: Frozen stock of rMOG(1-117) was streaked onto LB Kanamycin (30ug/ml) and ampicillin (100ug/ml) plates and grown overnight. Three ml of LB were inoculated with 3ul Kanamycin (30mg/ml stock) and 3ul Ampicilinin (100mg/ml stock) along with several colonies of E. coli. The culture was grown at 37° for 1.5 hrs. 1.5 ml of this stock was added into 500 ml LB with 500ul Kanamycin (30mg/ml stock) and 500ul Ampicilin (100mg/ml stock) and grown to an absorbance value at 600 nm of 0.6 – 0.8 (about 4 hours). 5ml of 100mM IPTG was added to induce protein expression to a final concentration of 1 mM and the culture grown at 16° overnight, then centrifuged at 2600g and 4° for 15 min. The supernatant was removed and frozen. 50 ml sonication buffer (100mM Tris, 1M NaCl, 10mM imidazole containing Complete EDTA free tablet (1 tablet/50ml) and PMSF (0.5ml/50ml)) was added to the pellet from two liters of growth. The sample was kept on ice for 1 hour and briefly

sonicated about every 10 minutes, then centrifuged at 13,000 rpm for 30 min to remove cellular debris. The supernatant was added to 3 ml Nickel resin (washed 2 times in buffer) and the protein was allowed to bind in the cold on a rocker for 2 hours. The slurry was then poured into a column and the flow through collected. The nickel-packed column was then washed with 30 ml of 10mM imidazole sonication buffer, followed by a wash with 30 ml of 30mM imidazole sonication buffer. The protein was eluted with 90mM imidazole sonication buffer as 10 - 2ml fractions and then checked on 15% SDS gel.

Sequence Analysis of Marmoset (C. jacchus) MOG (extracellular domain): The nucleotide sequence of marmoset MOG was determined by direct DNA sequencing of PCR products. Total RNA was extracted from C. jacchus lumbar and thoracic spinal cord in TRIzol (Gibco BRL). The first strand of cDNA was synthesized by RT-PCR in a final reaction volume of 10 µl containing 0.1 µg of total RNA, 1 mM dNTPs (Perkin Elmer), 0.25 units random hexamer primers (Pharmacia, Piscataway, NJ), 20 units human placental RNAse inhibitor (Gibco BRL), 100 units Superscript reverse transcriptase (Gibco), and 1 µl 10x PCR buffer (100 mM TRIS-Cl pH 8.3, 500 mM KCl, 15 mM MgCl2, 0.01% (w/v) gelatin (Perkin Elmer, Norwalk, CT). The reaction mixture was incubated for 10 minutes at room temperature, then for 45 minutes at 42 °C followed by 5 min at 95 °C and finally chilled on ice. The cDNA was amplified by 25 cycles of PCR with 10 µl of the reverse transcriptase reaction mixed in 50 µl final volume with 4 µl 10x PCR buffer and 0.5 µmol/l of the 3' MOG primer 5'GGGCAGTTCAGAGTGATA3'), in a "Hot Start" PCR reaction using 1.25 units of Tth XL polymerase (Perkin Elmer) and 0.5 µmol of the 5' primer 5'GCTCGAAGTTTTCCTCACAGT3'). Primers were based on human MOG cDNA sequences in the conserved amino acid regions across species (47-49). Fresh PCR products were cloned separately into PCR 2.1 cloning vector (TOPO Cloning Kit, Invitrogen) using the manufacturer's protocol. Ten positive clones were isolated from LB-agar plate and plasmids from each clone were obtained using centrifugation miniprep kits. Plasmids were then digested with EcoR1 and sized-separated on 1.0% agarose gels for detection of plasmids containing the PCR product insert. Plasmids containing the MOG (1-117) insert were sequenced using dideoxy chain-termination method following fmol sequencing kit protocol (Promega).

Circular Dichroism Experiments: The effects of different solvents, pH and temperature values on the stability and secondary structure of MOG(1-117) were monitored by CD using a Jasco 710 spectropolarimeter. CD spectra were acquired for 0.1 mg/ml MOG(1-117) from 25 °C to 90 °C in 5 degree steps. The CD spectrum of the corresponding buffer was subtracted from that of the protein and the spectra were analyzed by a backpropagation neural network algorithm using the program Circular Dichroism Deconvolution (http://bioinformatik.biochemtech.uni-halle.de/cdnn/).

Nuclear Magnetic Resonance (NMR) spectroscopy: Solution state NMR data at 25 °C were obtained using a 600 MHz Varian INOVA spectrometer. Gradient and sensitivity enhanced ^{15}N-^{1}H HSQC (heteronuclear single quantum correlation) (52) spectra were acquired on ~ 0.28 mM of MOG(1-117) dissolved in 50 mM of sodium d_3-acetateand 0.14 mM MOG(1-117) dissolved in 90%/10% H_2O/D_2O, pH 6.5. Two-dimensional ^{15}N-filtered 100 ms NOESY (nuclear Overhauser effect spectroscopy) spectra were acquired for 1 mM rat MOG(1-117) in 5 mM sodium acetate, pH 5.2 (53). ^{1}H and ^{15}N axes were referenced with respect to the dimethyl silapentane sulfonate (DSS) signal at 25 °C and indirectly to DSS using the ratio of gamma's (Hγ/Cγ or Hγ/Nγ), respectively (54). Spectra were processed and analyzed using the program FELIX (Aceryls, San Diego, CA). Both through bond TOCSY (Total correlation spectroscopy, 40 and 80 ms spin times) and through space NOESY (100 and 200 ms mixing times) data sets were collected on 0.1 mM MOG(122-150) (transmembrane domain) dissolved in deuterated DMSO.

Solid state NMR spectroscopy was performed at 25 °C using either a 500 MHz Bruker DRX spectrometer and a 4mm CPMAS probe or at 300 MHz Chemagnetics CMX spectrometer using a Doty Scientific flat coil probe. ^{13}C-^{13}C correlation experiments were performed according to previously published methods (106, 107). PISEMA experiments were performed as described previously (108).

Results

I. Extracellular domain characterization

Homology Modeling: A homology modeling study of human MOG(2-120) based on the crystal structure of myelin P0 predicts that the protein adopts an Ig type v-Greek key fold which consists of two β-sheets tightly packed together to form a sandwich. The 35% sequence homology and 55% predicted structural homology between human MOG(1-120) and P0 results in regions that have high prediction confidence. Thus, in the absence of experimentally determined structures, the model of human MOG(2-120) may be useful in the rational design of inhibitors against myelin/antibody interactions implicated in demyelinating disorders such as MS. The overall topology and global fold of the model agrees reasonably well with a previous model constructed of mouse MOG(1-121), although the details in the less conserved regions do not agree exactly (Fig. 2). Both models describe rational locations for a possible glycosylation site, dimerization surface, complement and antibody binding regions. In addition, potential phosphorylation sites have been identified.

The species-dependent fine T- and B-cell epitope specificities from MOG immunized rats and marmosets are compared and those from the marmosets are mapped onto the model of human MOG(2-120). The fine epitope specificities are predominately located in the A', C, and D strands and B-C and C"-D loops. It is not surprising to find that B cell and T cell responses to MOG are more diverse in non-human primates than in inbred strains of laboratory rodents. A diverse repertoire of responses to a major T cell antigen of myelin, myelin basic protein, has also been reported in primates, including the *C. jacchus* marmoset (Tabira & Kira, 1992; Genain *et al.*, 1995). Perhaps more relevant to MS and the model presented here, are the findings that marmosets and humans share common epitope regions that are targeted by both B cell and T cell responses to MOG (Kerlero de Rosbo *et al.*, 1997; Koehler *et al.*, 1997; Genain *et al.*, 1999). The C"-D loop (mouse model), or edge of C"-D loop-D-strand (human model) corresponds to T- and B-cell binding epitope sequences in rat MOG immunized marmosets and form a putative C1q binding site (residues 64-68), which may directly activate the classic complement pathway (Johns & Bernard, 1997). These regions are predominantly solvent exposed in

the monomeric form of the human MOG model and thus accessible to antibody or proteolytic attack.

Both the mouse and human MOG homology models predict a hydrophobic and aromatic surface for the A'-G-F-C-C'-C" sheet that may promote dimerization in aqueous environments. However, it is unknown whether MOG exists as a dimer *in vivo*, especially since it is a minor component of the myelin membrane comprising only 0.01 to 0.05% of the CNS myelin proteins. If MOG does exist as a dimer *in vivo* or if its monomeric form is associated with hydrophobic membrane constituents, such as lipids, cholesterol, or other myelin proteins, then access to the epitope sites located on the putative dimer interface would be hindered. In these cases, a change in the membrane environment or in the protein conformation would expose buried epitopes that may trigger or modulate pathogenic autoimmune responses in the disease-state. An alternative possibility is that post-translational modifications, such as glycosylation or phosphorylation would make the protein more soluble and thereby allow the exposure of hydrophobic surfaces in the monomeric form of the protein. Further studies are needed to investigate these possibilities and other proposed mechanisms for the immunopathogenesis of diseases such as MS.

Marmoset Epitope Specificities and Accessibility to Antibodies against MOG: C. jacchus marmosets sensitized to recombinant rat MOG (1-117) develop an antibody-mediated form of demyelination that is highly reminiscent of human MS (32). The fine specificity of B cell (antibody) and T cell immune responses have been identified in marmosets with the use of short overlapping peptides. Distinct marmoset B cell epitopes are found at residues 13-21 (10 of 10 animals), 28-35 (2 of 10 animals), 40-45 (3 of 10), 65-75 (6 of 10 animals). The minimal sequences necessary for peptide recognition by marmoset serum antibodies that are recognized by more than 60% of animals studied (major antibody epitopes) are residues 16-18 and 67-73. The major antibody epitopes are located on the opposite surfaces in the model (residues 16-18 on A' strand and A'-B loop are on the A'-G-F-C-C'-C" sheet while residues 67-73 on the D strand are on the A-B-E-D sheet. The other "minor", e.g. less frequently detected, antibody epitopes are located on the B-C loop (residues 28-35) and on the C strand and C-C' loop (residues 40-45).

The fine specificity of T cell epitopes could be determined in 8 animals. Particularly striking are the locations of the T cell epitopes with the major epitope residing in the CDR1 (B-C loop) site which spans the two sheets and the minor epitope encompassing the putative Cq1 (C"-D loop, D strand) binding site located on the A-B-E-D sheet. Most of these residues are located in regions that are solvent exposed; thus, these residues not only are potentially exposed to antibody attack, but are also readily accessible at the outer surface of the MOG molecule for binding of B cell surface immunoglobulins, a prerequisite for antigen recognition and presentation.

Activity Studies: Reactivity of the MOG(1-120) was studied. The results for MOG reactivity recombinant with (A) the recombinant monoclonal, MOG-specific marmoset Fab fragment M26, (B) serum from MOG-immune marmoset U013-99, and (C) the murine monoclonal antibody 8.18.C5 are shown in Figure 3. The data suggest that M26 and 8.18.C5 exclusively recognize conformational determinants of the folded MOG protein. Further, reactivity of MOG-immune marmoset serum against the soluble MOG recombinant (Liv-MOG=rMOG(1-117)) and the reference recombinant MOG used for immunization (rMOG) was tested (see Figure 4). These results show that the MOG expressed here and used in further structural studies was biologically active.

Solvent dependent secondary structure: MOG is an integral membrane protein and it is not known whether the extracellular domain is associated with the membrane or if its surface is fully solvent accessible. MOG(1-117) displays limited solubility in aqueous solutions and contains a large number of hydrophobic residues (56/120) in its amino acid sequence, some of which are predicted to lie on the edges between the two β-sheets and on the surface of the A'-G-F-C-C'-C" sheet. Biochemical studies (65-70), and ultrastructural characterization of CNS myelin (7, 32) indicate that the myelin composition undergoes major alterations in MS and EAE. Thus it is important to characterize MOG(1-117) under various solvent conditions not only to identify suitable conditions for structural studies, but also to better understand how in vivo environments, especially differences between the normal and disease states, can affect this protein's physical characteristics. Circular Dichroism (CD) is a technique that can monitor the

secondary structure conformation of MOG under various solvent conditions. We have used CD to estimate the % a-helix motif in the sectondary structure as a function of solution composition. Some example results are also shown in Figure 5.

In addition, we have initiated ^{15}N-^{1}H HSQC solution state NMR experiments on MOG(1-120) in a variety of solvent systems. An example is shown in Figure 6. It is expected that these experiments will shown the solvent induced conformation changes revealed in the CD studies in atomic level detail. Such studies are key to uncovering the origins of MOG pathogenisis.

Solution Additive	Relative mole α-helix
Dodecylphosphocholine (DPC)	9
Palmitoyllysophosphocholine (LPCP)	9
Palmitoyllysophosphatidic acid (LPAP)	15
Sodium lauryl sulfate (SDS)	12
45 % Trifluoroethanol (TFE)	20
No additive	9

Table 1. Relative mole percent of α helicity in rMOG[1-117] in the presence of detergents or TFE at 25°C, pH 7.5, in 10 mM phosphate buffer containing 5 mM β mercaptoethanol.

II. Transmembrane domain structure.

NOESY experiments of transmembrane domain: The ^{1}H NOESY spectrum of the transmembrane domain of MOG(122-150) in DMSO is shown in Figure 7. DMSO is often chosen as a initial solvent for transmembrane proteins because it is nonpolar, similar to the environment within the interior of the lipid environment of cell membranes. A ^{1}H TOCSY spectrum is shown in Figure 8 and the ^{13}C-^{1}H HMQC spectrum is shown in Figure 9. The Chemical shift index (CSI) plot for all the Cα chemical shifts in the

transmembrane domain (122-150) is shown in Figure 10. The data shown in Figures 7-10 indicates the majority of residues in this assigned segment assume a random coil status in DMSO. It is unlikely that this random coil structure is the actual structure found in membrane systems and further studies of this domain in micells and lipid bicelles (a amphiphile membrane simulant [109]) have been initiated to assess the structure of the transmembrane domain in a more cellular like environment.

Solid state NMR experiments: Currently, there are two methods to structurally characterize aqueous soluble proteins: solution state NMR spectroscopy and X-ray diffraction. However, structural characterizations of aqueous insoluble membrane proteins are difficult to obtain using these techniques. The rotational correlation times of membrane proteins dissolved in lipid-mimicking solvents are typically long, resulting in broad signals in the solution state NMR spectra. Further, membrane proteins are notoriously difficult to crystallize often preventing high-resolution XRD structures from being obtained

Fortunately, solid state NMR (SS-NMR) spectroscopy is not limited by the requirement to have soluble or crystallizable proteins. SS-NMR has provided detailed molecular level understanding of the structures and dynamics of both organic and inorganic macromolecules in the solid state. This advantage of SS-NMR is primarily due to the sensitivity of SS-NMR observables to anisotropic interactions that are functions of orientation and distance. In particular, the homo- and heteronuclear dipolar couplings and the chemical shift anisotropies of the nuclear moments are functions of the orientations ($\Omega(\theta,\phi,\gamma)$)of the relevant interaction frames with respect to the laboratory frame of reference [110]:

$$H_d = -(\mu_o/16\pi^2)h^2 \gamma_1 \gamma_2 \Sigma r_{ij}^{-3} (3\cos^2\theta - 1)(3I_zJ_z - \mathbf{I.J})$$

$$H_{cs} = \{\delta_{iso} \gamma B_o + 1/2\, \delta_{cs}[3\cos^2\theta - 1 - \eta_{cs} \sin^2\theta \cos^2\phi]\}$$

Where γ_1 and γ_2 are the gyromagnetic ratios of the nuclear moments of interest, r_{ij} is the distance between nuclear moments i and j, and θ and ϕ are the polar angles spanned by the interaction axis system and the laboratory axis defined by the applied magnetic field

and δ_{iso} and δ_{cs} are the isotropic and anisotropic parts of the chemical shift. In the case of the dipolar coupling interaction, the relevant interaction frame is coincident with the internuclear vector between nuclear moments. In the case of the chemical shift interaction, the interaction frame is rarely coincident with a specific bond but can be correlated to electron density around the nuclear moment. In short, measurement of these two observables will yield important structural constraints for the development of structural models.

Toward this end, we have initiated high resolution solid state NMR studies of the transmembrane domain of MOG (122-150). Method development was initated using three established methods: scalar coupling mediated homonuclear correlation experiements, dipolar coupling mediated homonuclear correlation experiments, and heteronuclear correlation experiments. The homonulcear correlation experiments were performed on a isotopically labeled sample of phenylanaline. Due to the low natural abundance of ^{13}C isotopes, in order to obtain high quality spectra in a reasonable amount of time, the investment in isotopic enrichment was necessary. The result of the scalar coupled ^{13}C-^{13}C homonuclear correlation experiment is shown in Figure 11. The standard 1D spectrum is shown along the horizontal axis while cross peaks along the vertical direction are the result of strong scalar (through bond) correlations between adjacent ^{13}C atoms. Of specific note is the increase in resolution in the aroamatic region of the spectrum (~120 ppm). In the 1D MAS spectrum shown above the 2D map, the aromatic region is comprised of 5 overlapping ^{13}C resonances with insufficient resolution to distinguish species. The 2D plot on the other hand, separates the spectral resonances by their next nearest neighbors and thereby increases the resolution. The use of these methods on a labeled protein such as MOG would allow for the assignments of resonances for further analysis for internuclear distance measurements.

We have, in addition, implemented a version of the ^{13}C-^{13}C correlation sequence to provide cross peak correlations via the dipolar coupling interactions which is directly related to internuclear distances (eq1). The result of this experiment is shown in Figure12. Here, the standard ^{13}C NMR spectrum is along the spectral diagonal and cross-peaks on the off-diagonal reflect the presence of dipolar coupling between sites. The intensity of the cross peaks is directly related to the internuclear distance between sites.

Experimental measurements of the internuclear distance provided acceptable agreement with the internuclear distance expected for a ^{13}C-^{13}C bond. The employment of such a method for ubiquitously labeled membrane proteins would allow for the direct measurement of internuclear distances in such systems and provide key structural insights.

Finally, we have implemented ^{15}N-^{1}H Polarization Inversion Spin Exchange at the Magic Angle (PISEMA) experiments. Such experiments provide orientation information for each residue in a peptide. Since, we were unable to obtain sufficiently ^{15}N labeled MOG(122-150) during the course of this LDRD, we chose to predict future experimental results based on expected orientation of an a-helix aligned 15 degrees off the membrane axis (which has been assigned parallel to the applied magnetic field) and with half of the nitrogen sites isotopically labeled with ^{15}N. The simulated PISEMA two dimensional experiment is shown in Figure 13 and shows the orientation dependent ^{15}N chemical shift in the horizontal dimension and the distance and orientation dependent ^{1}H-^{15}N dipolar coupling in the vertical dimension. The shape of the PISEMA wheel is a finger print of α-helix orientation. Similar PISEMA curves have been calculated for additional orientations and by comparison to experimental results, the exact orientation could be obtained.

CONCLUSIONS

We have constructed a three-dimensional model of human MOG(1-120) based on the analysis of immunoglobulin super family (IgSF) consensus residues and sequence-structure alignment with the high-resolution crystal structure of myelin P0 (*34*). Although the model can not predict the precise structure in regions of low sequence similarity, it should be sufficiently accurate to predict core and surface residues and their spatial arrangements. In addition, the molecular model of human MOG(1-120) is examined in light of CD, calorimetry and NMR experimental data obtained on rat MOG(1-117). Using the demyelinating model of EAE in the *C. jacchus* marmoset, we have identified the main encephalitogenic epitope sequences of rat MOG (1-117) in this species. Although EAE is efficiently induced in marmosets using rat MOG, due to close phylogeny, the *C. jacchus* marmoset MOG amino acid sequence is closer to that of human MOG rather than that of

the rat. Thus, we have mapped the fine T cell and B cell epitopes specificities identified in marmosets onto the homology model constructed for human MOG(1-120). The epitopes are found to be predominantly located on solvent exposed regions in the model and thus potentially accessible to antibody binding and/or proteolytic attack, which represent prerequisites for antigen recognition and processing by the immune system. Our experimental studies, in addition to providing evidence for our model, show that rat MOG(1-117) can readily adopt either the predicted β-sheet fold or a predominantly α-helical conformation dependent on the solvent conditions. To our knowledge, this is the first time that structural plasticity is demonstrated for an important autoantigen in an immune-mediated disorder. There is growing evidence that conformational instability may be more prevalent than previously suspected in promoting tissue damage in many neurological diseases, such as prion encephalopathies and Alzheimer's (*36*). Analogously, our data suggest that structural folding or misfolding of MOG(1-117) may also be an important factor in the immunopathogenesis of MS and related CNS demyelinating disorders.

Membrane proteins comprise approximately 30% of cellular proteins and are involved in critical functions such as signaling (communication between cells), mediating cell transport (including toxins), and within cell movement. Unfortunately, currently available methods are inadequate in determining the structures of membrane proteins and thus structure/function studies of this class of biomolecules are lagging behind those for their aqueous soluble counterparts. The research proposed here directly addresses this issue by proposing the development of new solid state NMR methods to study membrane proteins, such as MOG. The work will bring together the multidisciplinary expertise in BBRP on MOG and multiple sclerosis and in C&MS on solid state NMR methods development. The new techniques and tools for studying membrane proteins will provide fundamental knowledge about this important MS autoantigen, and provide the scientific community with a new powerful tool by which they can study other proteins, such as toxin receptors, with applications for the development of biosensors.

References:

1. Schappert, S. M. (1995) in *Vital and Health Statistics of the Centers for Disease Control and Prevention/National Center for Health Statistics* pp 1-20.
2. Martin, R., McFarland, H. F., and McFarlin, D. E. (1992) *Ann. Rev. Immunol. 10*, 153.
3. Oksenberg, J. R., Panzara, M. A., Begovich, A. B., Mitchell, D., Erlich, H. A., Murray, R. S., Shimonkevitz, R., Sherrity, M., Rothbard, J., Bernard, C. C. A., and Steinman, L. (1993) *Nature 362*, 68-70.
4. Hohlfeld, R., Londei, M., Massacesi, L., and Salvetti, M. (1995) *Immunol Today 16*, 259-61.
5. Zamvil, S. S., and Steinman, L. (1990) *Annu Rev Immunol 8*, 579-621.
6. Wekerle, H. (1993) *Curr Opin Neurobiol 3*, 779-84.
7. Brosnan, C. F., and Raine, C. S. (1996) *Brain Pathol 6*, 243-57.
8. Luchinetti, C., Bruck, W., Rodriguez, M., and Lassmann, H. (1996) *Brain Pathol. 6*, 259-274.
9. Hohlfeld, R. (1997) *Brain 120*, 865-916.
10. Linington, C., Engelhardt, B., Kapocs, G., and Lassman, H. (1992) *J Neuroimmunol 40*, 219-24.
11. Amor, S., Groome, N., Linington, C., Morris, M. M., Dornmair, K., Gardinier, M. V., Matthieu, J. M., and Baker, D. (1994) *J Immunol 153*, 4349-4356.
12. Johns, T. G., Derosbo, N. K., Menon, K. K., Abo, S., Gonzales, M. F., and Bernard, C. C. A. (1995) *J Immunol 154*, 5536-5541.
13. Genain, C. P., Nguyen, M. H., Letvin, N. L., Pearl, R., Davis, R. L., Adelman, M., Lees, M. B., Linington, C., and Hauser, S. L. (1995) *J Clin Invest 96*, 2966-74.
14. Sun, J. B., Link, H., Olsson, T., Xiao, B. G., Andersson, G., Ekre, H. P., Linington, C., and Diener, P. (1991) *J Immunol 146*, 1490-1495.
15. Xiao, B. G., Linington, C., and Link, H. (1991) *J Neuroimmunol 31*, 91-6.
16. Kerlero de Rosbo, N., Milo, R., Lees, M. B., Burger, D., Bernard, C. C. A., and Ben-Nun, A. (1993) *J. Clin. Invest. 92*, 2602-2608.
17. Reindl, M., Linington, C., Brehm, U., Egg, R., Dilitz, E., Deisenhammer, F., Poewe, W., and Berger, T. (1999) *Brain 122*, 2047-2056.
18. Schluesener, H. J., Sobel, R. A., Linington, C., and Weiner, H. L. (1987) *J. Immunol. 139*, 4016-4021.
19. Genain, C. P., and Hauser, S. L. (1996) *10*, 420-434.
20. Amiguet, P., Gardinier, M. V., Zanetta, J. P., and Matthieu, J. M. (1992) *J Neurochem 58*, 1676-1682.
21. Linington, C., Webb, M., and Woodhams, P. L. (1984) *J. Neuroimmunol. 6*, 387-396.
22. Brunner, C., Lassmann, H., Waehneldt, T. V., Matthieu, J.-M., and Linington, C. (1989) *J. Neurochem. 52*, 296-304.
23. Johns, T. G., and Bernard, C. C. A. (1999) *J. Neurochem. 72*, 1-9.

24. Linsley, P. S., Peach, R., Gladstone, P., and Bajorath, J. (1994) *Protein Sci 3*, 1341-3.
25. Henry, J., Ribouchon, M. T., Offer, C., and Pontarotti, P. (1997) *Biochem Biophys Res Commun 235*, 162-5.
26. Kroepfl, J. F., Viise, L. R., Charron, A. J., Linington, C., and Gardinier, M. V. (1996) *J Neurochem 67*, 2219-2222.
27. Della Gaspera, B., Pham-Dinh, D., Roussel, G., Nussbaum, J. L., and Dautigny, A. (1998) *Eur J Biochem 258*, 478-484.
28. Adelmann, M., Wood, J., Benzel, I., Fiori, P., Lassmann, H., Matthieu, J. M., Gardinier, M. V., and Dornmair, K. (1995) *J Neuroimmunol 63*, 17-27.
29. Mendel, I., Derosbo, N. K., and Bennun, A. (1995) *Eur J Immunol 25*, 1951-1959.
30. Ichikawa, M., Johns, T. G., Adelmann, M., and Bernard, C. C. A. (1996) *Int Immunol 8*, 1667-1674.
31. Kerlero de Rosbo, N., Hoffman, M., Mendel, L., Yust, I., Kaye, J., Bakimer, R., Flechter, S., Abramsky, O., Milo, R., Karni, A., and Ben-Num, A. (1997) *Eur. J. Immunol. 27*, 3059-3069.
32. Raine, C. S., Cannella, B., Hauser, S. L., and Genain, C. P. (1999) *Ann Neurol 46*, 144-160.
33. Genain, C. P., Cannella, B., Hauser, S. L., and Raine, C. S. (1999) *Nature Med 5*, 170-175.
34. Shapiro, L., Doyle, J. P., Hensley, P., Colman, D. R., and Hendrickson, W. A. (1996) *Neuron 17*, 435-49.
35. Hjelmstrom, P., Penzotti, J. E., Henne, R. M., and Lybrand, T. P. (1998) *J Neurochem 71*, 1742-1749.
36. Carrell, R. W., and Gooptu, B. (1998) *Curr Opin Struct Biol 8*, 799-809.
37. Altschul, S. F., Gish, W., Miller, W., Myers, E. W., and Lipman, D. J. (1990) *J Mol Biol 215*, 403-10.
38. Corpet, F., Gouzy, J., and Kahn, D. (1998) *Nucleic Acids Res 26*, 323-6.
39. Rost, B., and Sander, C. (1993) *Proc Natl Acad Sci U S A 90*, 7558-62.
40. Rost, B., and Sander, C. (1993) *J Mol Biol 232*, 584-99.
41. Rost, B., and Sander, C. (1994) *Proteins 20*, 216-26.
42. Rost, B., Sander, C., and Schneider, R. (1994) *Comput Appl Biosci 10*, 53-60.
43. Geourjon, C., and Deléage, G. (1995) *Comput Appl Biosci 11*, 681-4.
44. Sander, C., and Schneider, R. (1991) *Proteins 9*, 56-68.
45. Laskowski, R. A., Rullmannn, J. A., MacArthur, M. W., Kaptein, R., and Thornton, J. M. (1996) *J Biomol NMR 8*, 477-86.
46. Dyall, K. G., Grant, I. P., Johnson, C. T., Parpia, F. A., and Plummer, E. P. (1989) *Comput Phys Commun 55*, 425-456.
47. Gardinier, M. V., Amiguet, P., Linington, C., and Matthieu, J. M. (1992) *J Neurosci Res 33*, 177-87.

48. Pham-Dinh, D., Allinquant, B., Ruberg, M., Dellagaspera, B., Nussbaum, J. L., and Dautigny, A. (1994) *J Neurochem 63*, 2353-2356.

49. Phamdinh, D., Dellagaspera, B., Derosbo, N. K., and Dautigny, A. (1995) *Genomics 29*, 345-352.

50. Genain, C. P., Abel, K., Belmar, N., Villinger, F., Rosenberg, D. P., Linington, C., Raine, C. S., and Hauser, S. L. (1996) *Science 274*, 2054-7.

51. Geysen, H. M., Rodda, S. J., Mason, T. J., Tribbick, G., and Schoofs, P. G. (1987) *J Immunol Methods 102*, 259-74.

52. Kay, L. E., Keifer, P., and Saarinen, T. (1992) *J Amer Chem Soc 114*, 10663-10665.

53. Talluri, S., and Wagner, G. (1996) *J Magn Resonance Ser B 112*, 200-205.

54. Bax, A., and Subramanian, S. (1986) *J. Magn. Reson. 67*, 565-569.

55. Wu, D. H., Chen, A. D., and Johnson, C. S. (1995) *J Magn Resonance Ser A 115*, 260-264.

56. Mescher, M., Tannus, A., Johnson, M. O., and Garwood, M. (1996) *J Magn Resonance Ser A 123*, 226-229.

57. Krishnan, V. V., Thornton, K. H., and Cosman, M. (1999) *Chem Phys Lett 302*, 317-323.

58. Garcia de la Torre, J. G., and Bloomfield, V. A. (1981) *Q Rev Biophys 14*, 81-139.

59. Orekhov, V. Y., Nolde, D. E., Golovanov, A. P., Korzhnev, D. M., and Arseniev, A. S. (1995) *Appl Magn Reson 9*, 581-588.

60. Chothia, C., Gelfand, I., and Kister, A. (1998) *J Mol Biol 278*, 457-79.

61. Johns, T. G., and Bernard, C. C. A. (1997) *Mol Immunol 34*, 33-38.

62. Gerstein, M., Tsai, J., and Levitt, M. (1995) *J Mol Biol 249*, 955-66.

63. Bairoch, A., Bucher, P., and Hofmann, K. (1997) *Nucleic Acids Res 25*, 217-21.

64. Rudd, P. M., and Dwek, R. A. (1997) *Crit Rev Biochem Mol Biol 32*, 1-100.

65. Allen, I. V., and McKeown, S. R. (1979) *J Neurol Sci 41*, 81-91.

66. Husted, C. A., Goodin, D. S., Hugg, J. W., Maudsley, A. A., Tsuruda, J. S., de Bie, S. H., Fein, G., Matson, G. B., and Weiner, M. W. (1994) *Ann. Neurol. 36*, 157-165.

67. Husted, C. A., Matson, G. B., Adams, D. A., Goodin, D. S., and Weiner, M. W. (1994) *Ann Neurol 36*, 239-241.

68. Boggs, J. M., Rangaraj, G., Koshy, K. M., Ackerley, C., Wood, D. D., and Moscarello, M. A. (1999) *J Neurosci Res 57*, 529-35.

69. Ohler, B., Graf, K., Lemons, T., Coe, R., Jahangir, S., See, W., Genain, C., and Husted, C. (1999) *J. Neurochem. 72*, (Suppl.):S15D.

70. Trapp, B. D., Bo, L., Mork, S., and Chang, A. (1999) *J Neuroimmunol 98*, 49-56.

71. Carpenter, K. A., Wilkes, B. C., De Léan, A., Fournier, A., and Schiller, P. W. (1997) *Biopolymers 42*, 37-48.

72. Kuwata, K., Hoshino, M., Era, S., Batt, C. A., and Goto, Y. (1998) *J Mol Biol 283*, 731-9.

73. Birling, M. C., Roussel, G., Nussbaum, F., and Nussbaum, J. L. (1993) *Neurochem Res 18*, 937-945.

74. Slavin, A. J., Johns, T. G., Orian, J. M., and Bernard, C. C. A. (1997) *Develop Neurosci 19*, 69-78.
75. Teller, D. C., Swanson, E., and de Haën, C. (1979) *Methods Enzymol 61*, 103-24.
76. Krishnan, V. V. (1997) *J Magn Reson 124*, 468-473.
77. Griffith, L. S., Schmitz, B., and Schachner, M. (1992) *J Neurosci Res 33*, 639-48.
78. Burger, D., Steck, A. J., Bernard, C. C. A., and Derosbo, N. K. (1993) *J Neurochem 61*, 1822-1827.
79. Quarles, R. H. (1997) *J Mol Neurosci 8*, 1-12.
80. Tabira, T., and Kira, J.-I. (1992) in *Myelin: Biology and Chemistry* (Martenson, R. E., Ed.) pp 783-799, CRC Press, Inc., Boca Raton, Fl.
81. Koehler, N., Shao, L., Genain, C., and Hauser, S. (1997) *Ann. Neurol. 42*, 458.
82. Stevens, B. R., Raizada, M., Sumners, C., and Fernandez, A. (1987) *Brain Res 406*, 113-7.
83. Bever, C. T., Jr., and Garver, D. W. (1995) *J Neurol Sci 131*, 71-3.
84. Vergelli, M., Kalbus, M., Rojo, S. C., Hemmer, B., Kalbacher, H., Tranquill, L., Beck, H., McFarland, H. F., De Mars, R., Long, E. O., and Martin, R. (1997) *J Neuroimmunol 77*, 195-203.
85. Johnson, R. T. (1994) *Ann Neurol 36*, S54-S60.
86. Dal Canto, M. C., Melvold, R. W., Kim, B. S., and Miller, S. D. (1995) *Microsc Res Tech 32*, 215-29.
87. Albouz-Abo, S., Wilson, J. C., Bernard, C. C. A., and von Itzstein, M. (1997) *Eur J Biochem 246*, 59-70.
88. Genain, C. P., Thornton, K., Krishnan, V. V., Mesleh, M. H., and Cosman, M. (2000) *Ann. Neurol. 46*, 936.
89. Roth, M. P., Dolbois, L., Borot, N., Pontarotti, P., Clanet, M., and Coppin, H. (1995) *J Neuroimmunol 61*, 117-122.
90. Helms, L. R., and Wetzel, R. (1995) *Protein Sci 4*, 2073-81.
91. Radford, S. E., and Dobson, C. M. (1999) *Cell 97*, 291-8.
92. Cordes, M. H. J., Walsh, N. P., McKnight, C. J., and Sauer, R. T. (1999) *Science 284*, 325-327.
93. Jackson, G. S., Hosszu, L. L. P., Power, A., Hill, A. F., Kenney, J., Saibil, H., Craven, C. J., Waltho, J. P., Clarke, A. R., and Collinge, J. (1999) *Science 283*, 1935-1937.
94. Svennerholm, L., Boström, K., and Jungbjer, B. (1997) *Acta Neuropathol (Berl) 94*, 345-52.
95. Koenig, H. L., Schumacher, M., Ferzaz, B., Thi, A. N., Ressouches, A., Guennoun, R., Jung-Testas, I., Robel, P., Akwa, Y., and Baulieu, E. E. (1995) *Science 268*, 1500-3.
96. Schumacher, M., Robel, P., and Baulieu, E. E. (1996) *Dev Neurosci 18*, 6-21.
97. Jung-Testas, I., Schumacher, M., Robel, P., and Baulieu, E. E. (1996) *J Steroid Biochem Mol Biol 58*, 77-82.
98. Guennoun, R., Schumacher, M., Robert, F., Delespierre, B., Gouézou, M., Eychenne, B., Akwa, Y., Robel, P., and Baulieu, E. E. (1997) *Eur J Neurosci 9*, 2236-47.
99. Runmarker, B., and Andersen, O. (1995) *Brain 118*, 253-61.

100. Minor, D. L., Jr., and Kim, P. S. (1996) *Nature 380*, 730-4.

101. Parker, W., and Stezowski, J. J. (1996) *Proteins 25*, 253-60.

102. Abrahamson, M., and Grubb, A. (1994) *Proc Natl Acad Sci U S A 91*, 1416-20.

103. Riek, R., Wider, G., Billeter, M., Hornemann, S., Glockshuber, R., and Wuthrich, K. (1998) *Proc Nat Acad Sci USA 95*, 11667-11672.

104. Koradi, R., Billeter, M., and Wüthrich, K. (1996) *J Mol Graph 14*, 51-5, 29-32.

105. Mesleh, M. F., Belmar, N., Lu, C.-W., Krishnan, V. V., **Maxwell, R. S.**, Genain, C. P., and Cosman, M. *Neurobiology of Disease* **9**, 160-172 (2002).

107. Jarrel, H. C., Lu, D., Siminovitch, D. J., J. Am. Chem. Soc. 1998, 120, 10453-10462.

106. Lessage, A., Bardet, M., Emsley, L., J Am. Chem. Soc. 1999, 121, 10987-10993.

108. Marassi, F., Opella, S. J., J. Mag. Res. 2000, 144, 150-155.

109. Prosser, R. S., Hunt, S. A., Vold R. R. (1995) *J. Mag. Res. B* **109**: 109-111.

110. Schmidt-Rohr, K., Spiess, H. W. (1994) Multidimensional Solid State NMR and Polymers. Academic Press, NY.

Figure 1: Putative topology of MOG

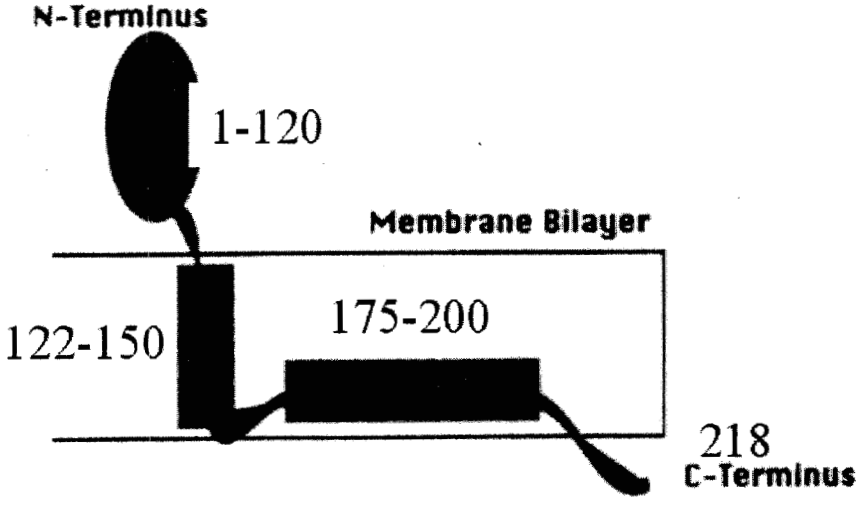

Figure 2. Results of homology modeling of the extracellular domain of MOG (1-120) for human an drat MOG. These are all of the human MOG model – A and C are showing one face – the ABED beta sheet side and B and D are showing a 180 degree rotation so that the other face – the A'GFCC'C" face is seen. A and B designate whether the surface residue is acidic, basic, hydrophobic or polar – C and D show the model represented in secondary structural elements – beta strands and loops – with the T-cell (green), B-cell (blue) and T and B-cell (yellow) epitopes designated.

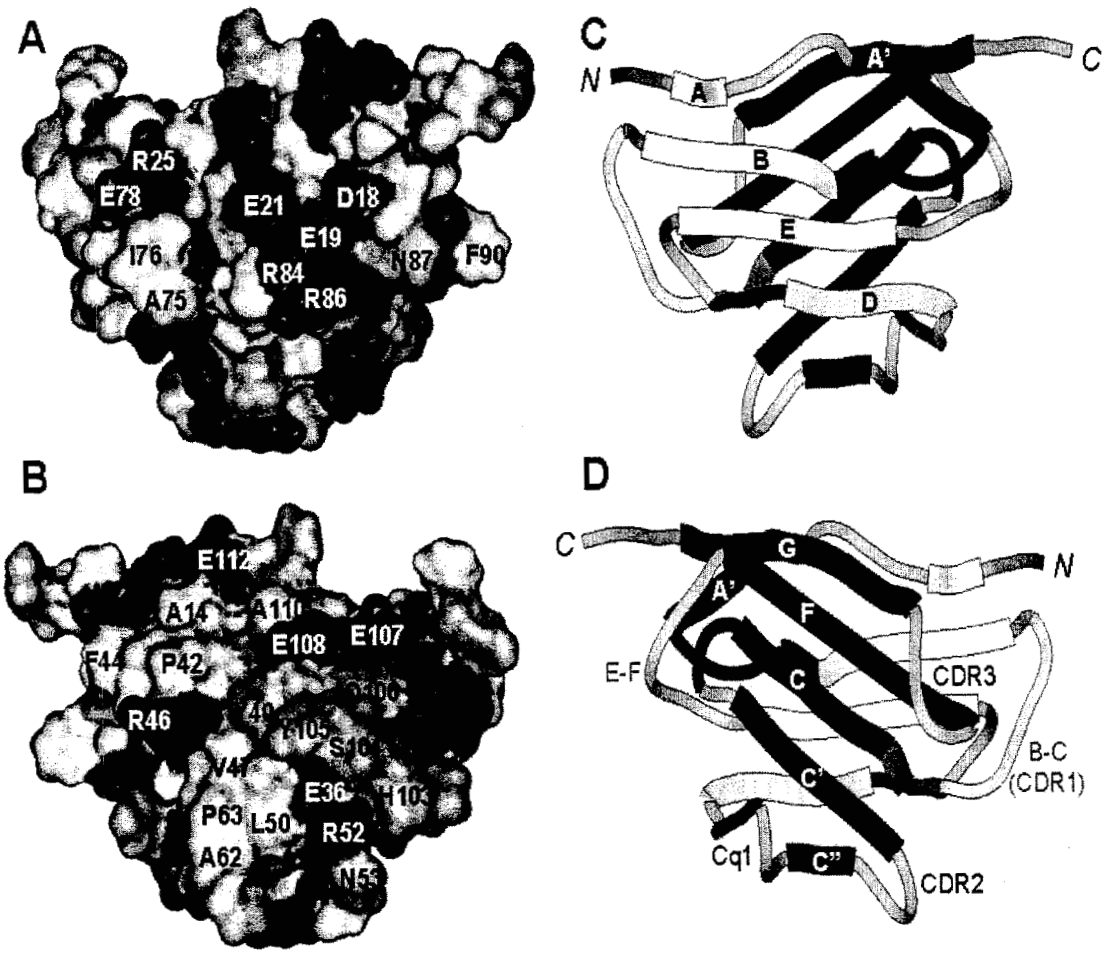

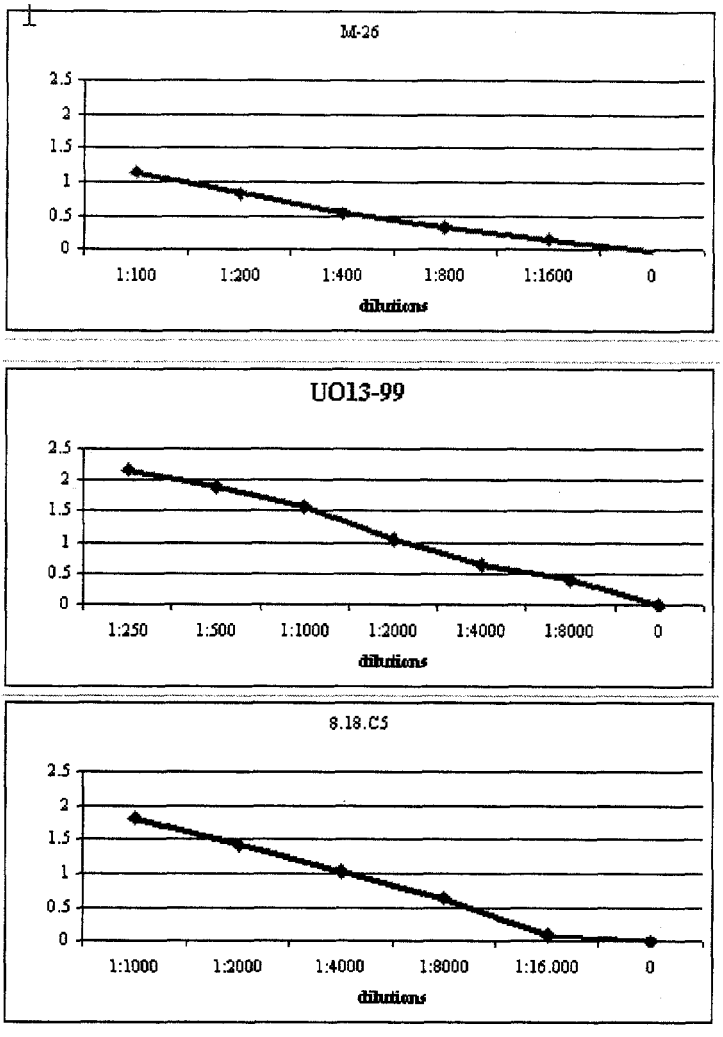

Figure 3. Reactivity of the soluble MOG recombinant with: the recombinant monoclonal, MOG-specific marmoset Fab fragment M26 (top); serum from MOG-immune marmoset U013-99 (middle); the murine monoclonal antibody 8.18.C5 (bottom). M26 and 8.18.C5 exclusively recognize conformational determinants of the folded MOG protein

Figure 4. . Reactivity of MOG-immune marmoset serum against the soluble MOG recombinant (Liv-MOG=rMOG(1-117)) and the reference recombinant MOG used for immunization (rMOG).

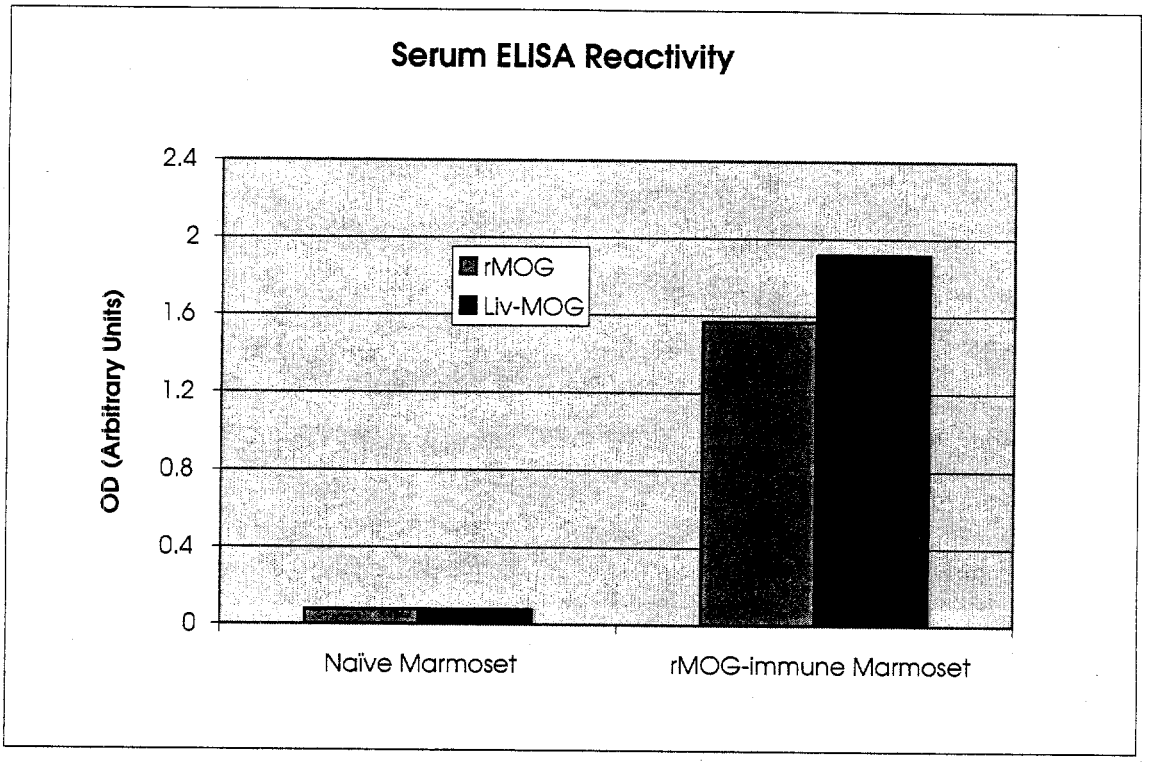

Figure 5. CD spectrum of rMOG[1-117] (0.17 mg/ml) in 10 mM phosphate at pH 7.5 at 25 °C, (·····) (β-form) and in the presence of 2 mM LPAP, (—) (α-form). A theoretical fit to the CD spectrum yielded ca. 9% α-helix and 38 % β-antiparallel sheet, and ca. 15 % % α-helix and 27 % β-antiparallel sheet, for the β-form and α-form, respectively.

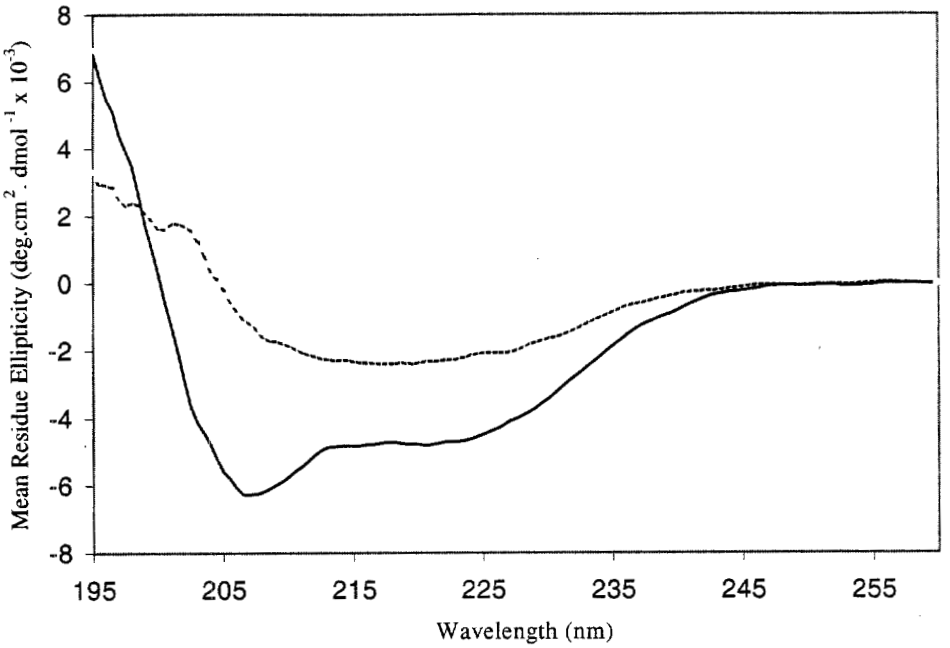

Figure 6. ^{15}N-^{1}H HSQC spectrum of the extracellular domain indicating that the extracellular domain in SDS buffer is either partially folded or two or more conformations are present.

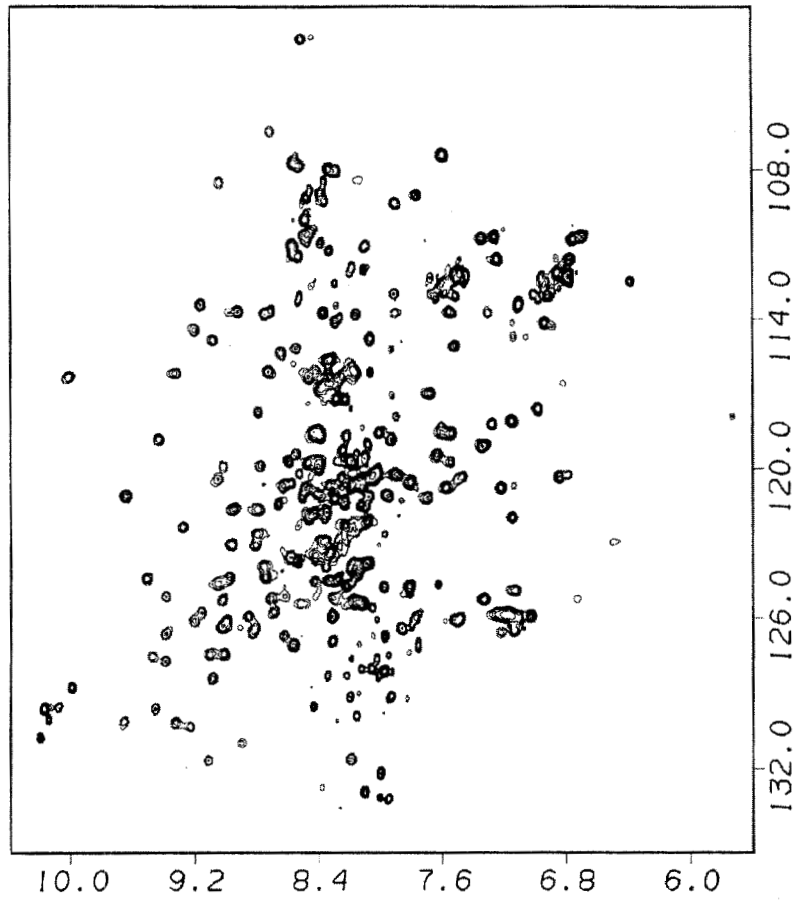

Figure 7. ^{1}H NOESY spectrum of transmembrane domain of MOG in DMSO.

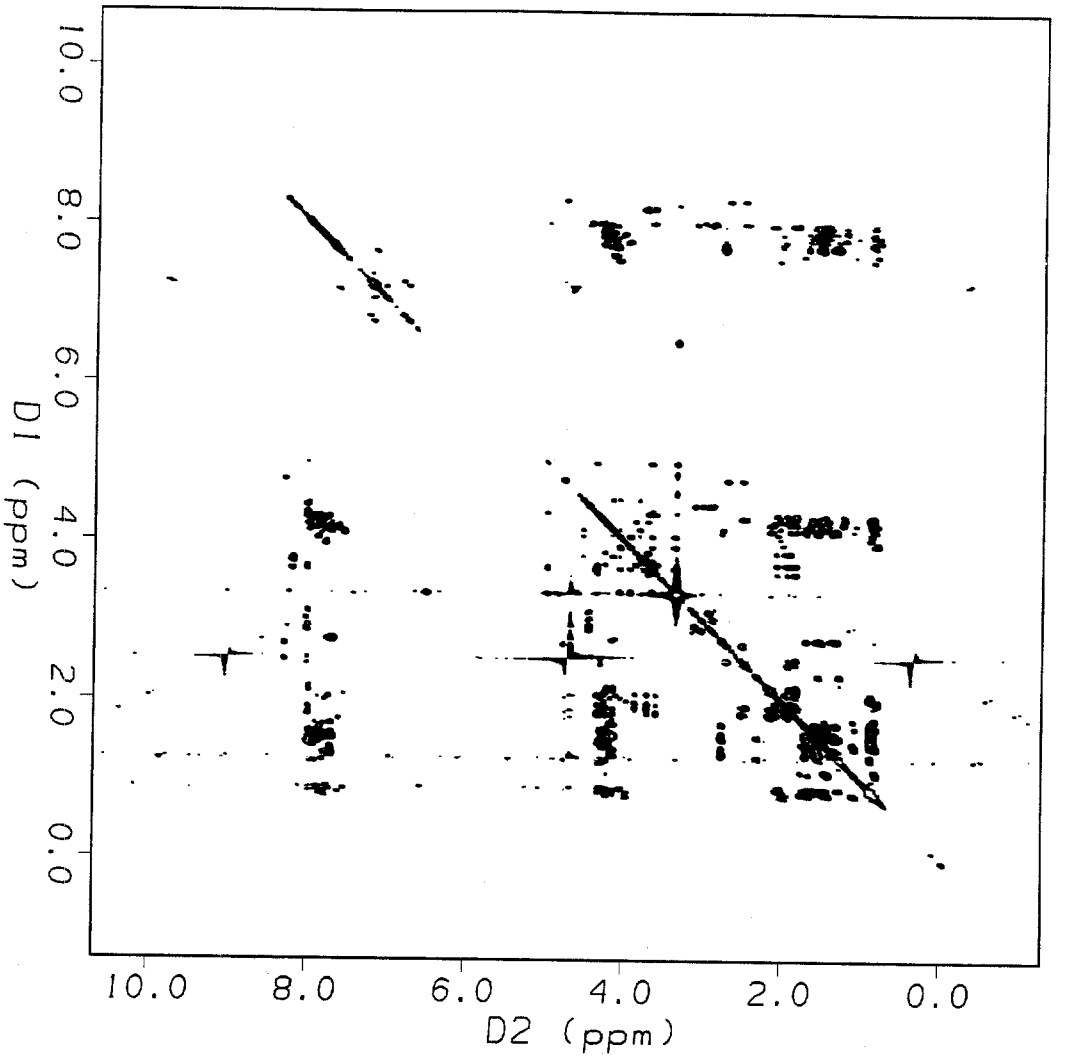

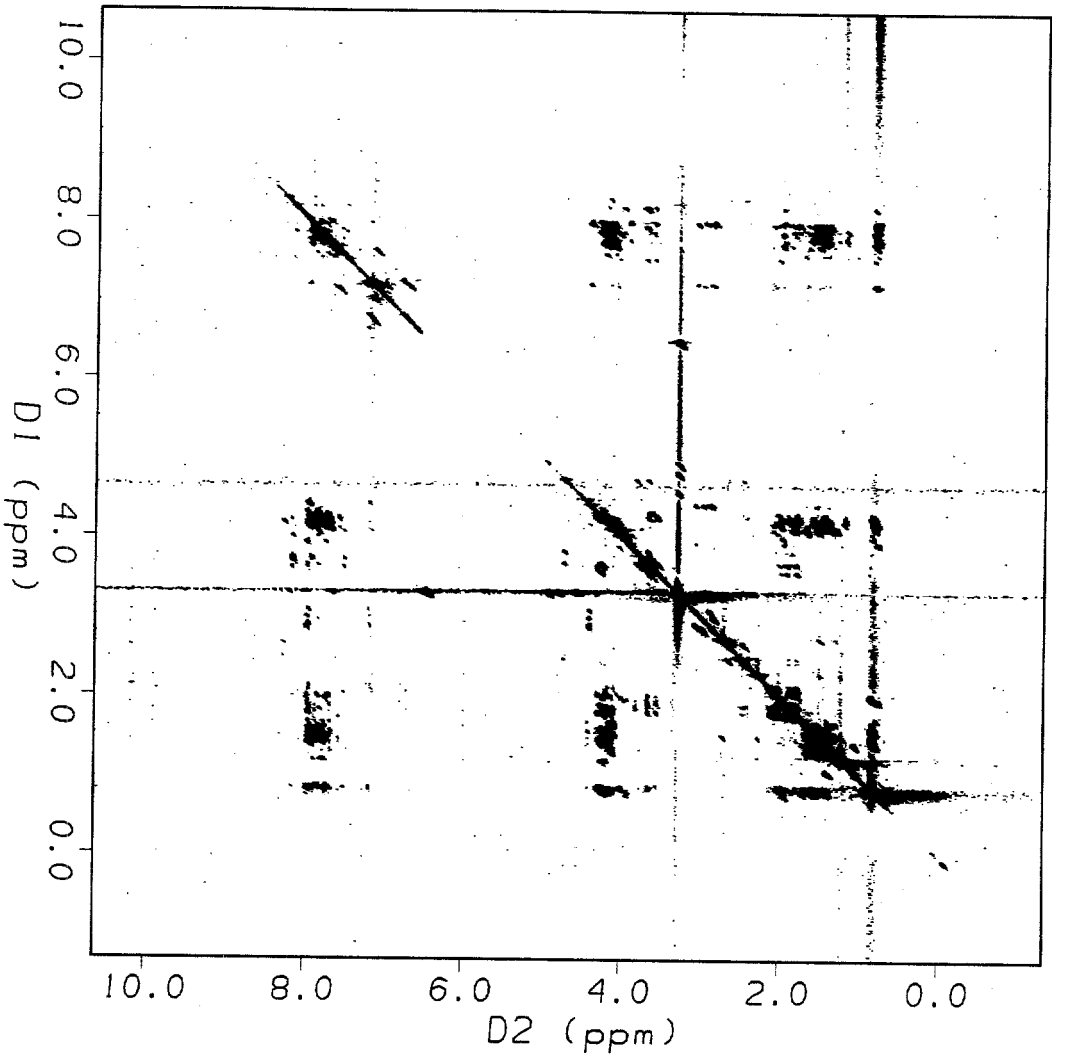

Figure 8. ^{1}H TOCSY spectrum of transmembrane domain of MOG.

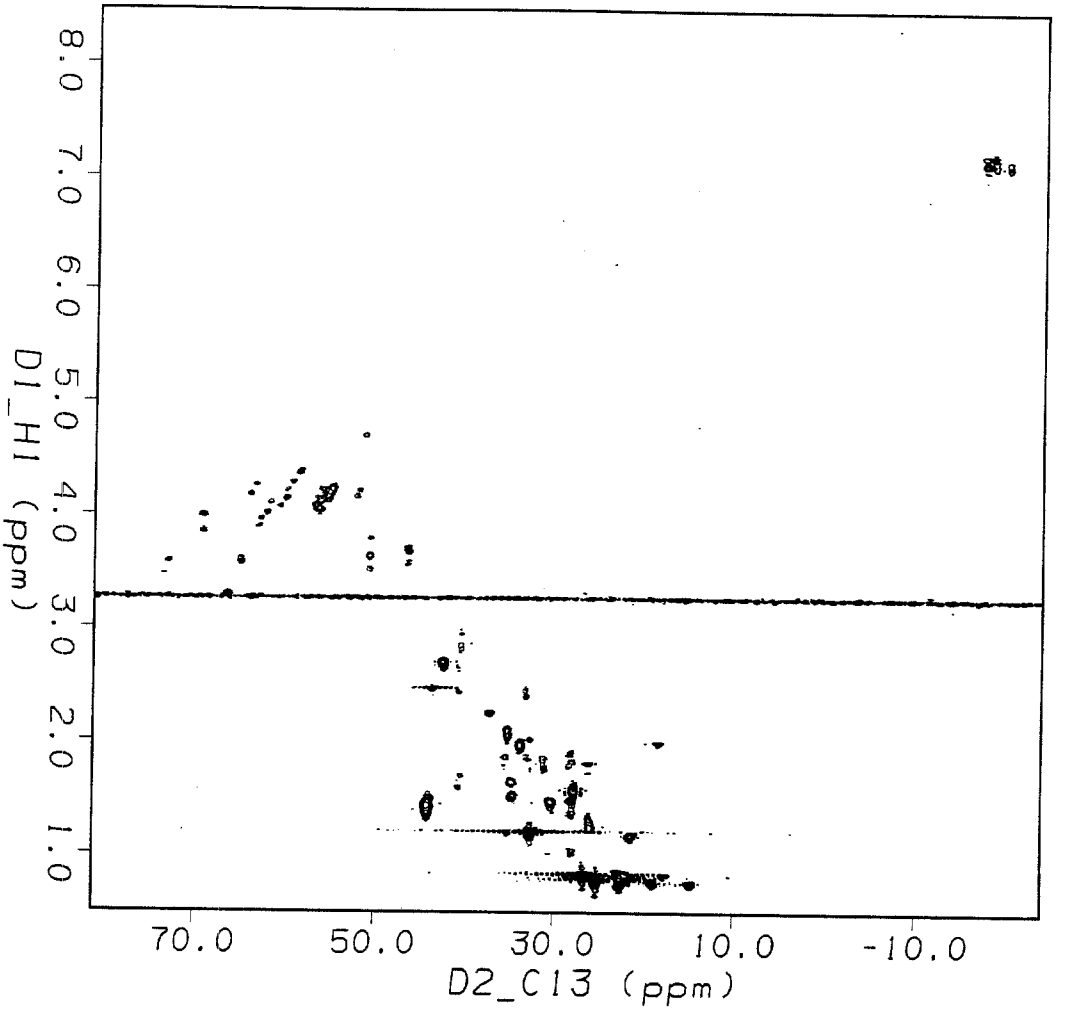

Figure 9. ^{1}H-^{13}C HMQC spectrum of MOG(122-150) in DMSO.

Figure 10. Chemical Shift Index plot for transmembrane domain of MOG in DMSO.

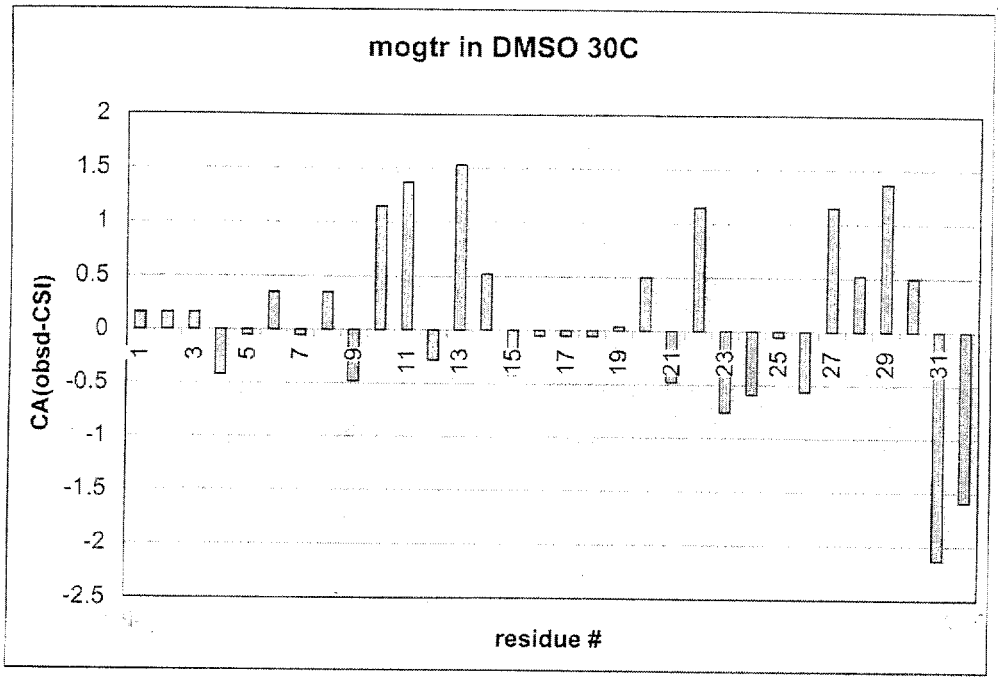

Figure 11. ^{13}C-^{13}C Scalar coupling mediated, double quantum homonuclear correlation spectrum.

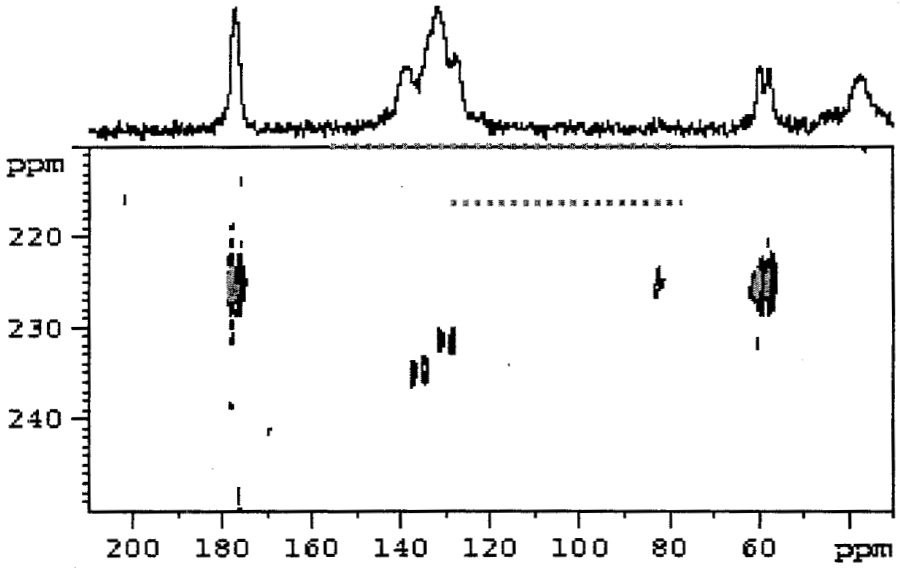

Figure 12. ^{13}C-^{13}C dipolar coupling mediated, signle quantum homonuclear correlation spectur.

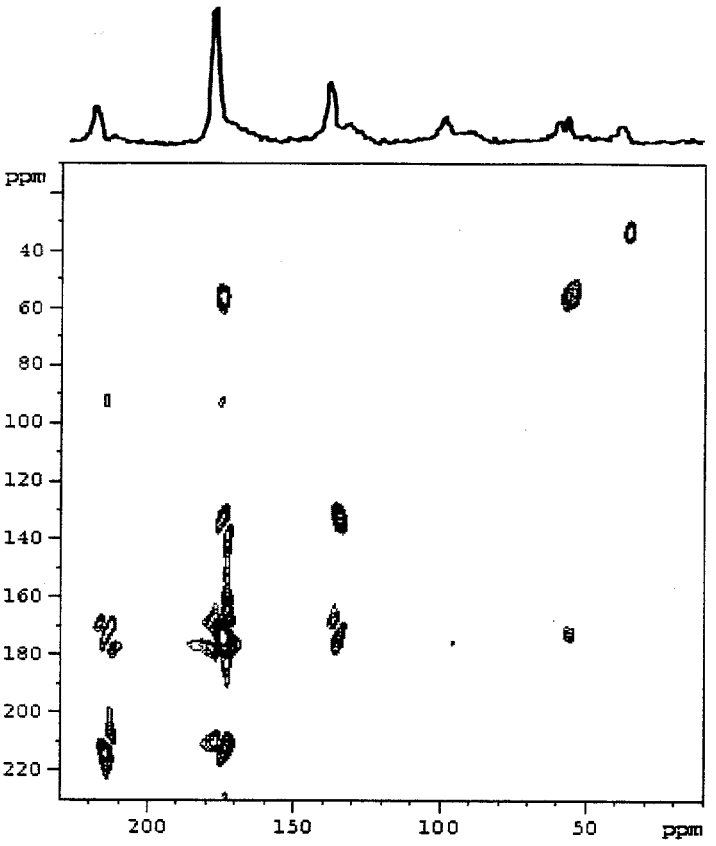

Figure 13. Computer generated ^{1}H-^{15}N PISEMA solid state NMR simulation for transmembrane domain of MOG.